DOI: 10.13009/EUCASS2023-504
Aerospace Europe Conference 2023 – 10TH EUCASS – 9TH CEAS

Sensor fault detection and isolation for electro-mechanical actuators in a reusable launch vehicle TVC system

Stefano Farì[⋆†], David Seelbinder[⋆], Stephan Theil[⋆], Pedro Simplicio[⋆⋆] and Samir Bennani[⋆⋆]

[⋆] *German Aerospace Center (DLR), Robert-Hooke-Str. 7, Bremen, Germany*
{Stefano.Fari, David.Seelbinder, Stephan.Theil} @dlr.de
[⋆⋆] *European Space Agency (ESA), Keplerlaan 1, Noordwijk, The Netherlands*
Pedro.Simplicio@ext.esa.int, Samir.Bennani@esa.int
[†]Corresponding author

Abstract

This paper introduces a model-based Fault Detection and Isolation (FDI) approach for a Reusable Launch Vehicle (RLV) Thrust Vector Control (TVC) system operated by Electro-Mechanical Actuators (EMAs). The focus is on the sensors required for the EMA embedded control system to track the on-board computer control commands. The nullspace FDI method is considered and applied to detect and isolate additive faults affecting the mentioned sensors. A detailed formulation of the problem and the EMA-based TVC system modelling for FDI synthesis is provided, including the mechanical load exerted by the rocket nozzle. The FDI synthesis framework is introduced and the application of the nullspace-based strategy is described, including considerations about isolability of the faults. Vehicle-induced loads can potentially disrupt the fault detection process, therefore they are included in the problem formulation to achieve decoupling from the residual generator output and not incur into false alarms. The generator performance is then assessed in fault-free and faulty scenarios using a high-fidelity TVC physical model, and successively benchmarked at the example of an RLV mission scenario.

1. Introduction

The R&D for Vertical Take-off Vertical Landing (VTVL) Reusable Launch Vehicles (RLV) is gaining a high momentum worldwide. In Europe, several technology demonstrators and commercial launchers are being developed, like CALLISTO,[1,2] Themis,[3] or RETALT;[4] on the other hand, the Ariane Next reusable launcher development program aims at achieving reusability in a commercial context. To bring RLV reliability to sufficient standards, suitable algorithms for fault handling and recovery from upset conditions must be investigated. As such, performing Fault Detection and Isolation (FDI) mechanisms are essential to let the onboard software gather awareness of an in-mission performance degradation. The reason why fault detection, diagnosis and recovery are relevant matters for these vehicles is that all mission phases pose harsh challenges to the vehicle's G&C since the performance requirements are usually very strict; as a consequence, any malfunction in a sensor or actuator, or an unforeseen vehicle structural change, could be disruptive, leading to mission degradation or to the loss of vehicle, even with a control system designed for the maximum achievable robustness. It is important therefore to provide software logic able to detect and diagnose a fault, which in turn can lead to an advantage if this additional knowledge is appropriately exploited. The engine's Thrust Vector Control system (TVC) is a critical vehicle control mean; to drive it, Electro-Hydraulic Actuators (EHAs)[5] or Electro-Mechanical Actuators (EMAs)[6] can be employed. The paper focuses on TVC systems based on EMAs. Electrical power drives are progressively tending to replace fluid power drives, especially in aeronautics where the goal is to achieve sufficient reliability for EMAs to completely remove the hydraulic actuators also for the primary control surfaces.[7–9] Launch vehicles can benefit of such an implementation because a large fraction of mass, space, and cost can be saved with respect to the more conventional hydraulic actuators.[5,10] Their applicability has been proven, for example, by the expendable European VEGA rocket[11–13] over two decades of operational life, or by the Electron rocket.[6]

Several measurements are necessary in EMAs for correct operation, and to comply with damping and response speed requirements. An LVDT[1] stroke displacement sensor, an electric motor encoder and a current sensor are normally

[1]Linear Variable Differential Transformer.

DOI: 10.13009/EUCASS2023-504

included; faults affecting these devices must be detected and counteracted, in order to accommodate the fault or switch to a redundant physical or virtual sensor for the purpose of not deteriorating the EMA closed-loop performance and preventing bad tracking of the nozzle deflection commands. This is also justified by the fact that EMAs cannot be easily switched to passive mode whenever they experience a physical fault, therefore it is reasonable to start the investigation from the sensor units, whose degradation can be very detrimental while the EMA is still mechanically fully operative. Several strategies to detect faults can be employed. Model-based FDI methods can be considered as more effective than signal-based or data-based techniques because they enable more types of faults to be addressed at the same time. They work by generating a residual signal as difference between measurements and the predictions of adequate mathematical models. These residuals can then be used to determine if a fault has occurred when compared to suitable thresholds.

1.1 State-of-the-art and objectives

Several model-based FDI techniques have been extensively studied over the last decades and applied to numerous problems. In classical hydraulic flight actuators, advanced methods have been proposed by Ossmann and Varga *et al.* using LPV techniques.[14–16] Ossmann *et al.* also introduce a sensor monitoring technique to solve the angle of attack sensor fault isolation problem for optimal aircraft handling.[14] Specifically for electro-mechanical actuators, Balaban *et al.* have proposed a diagnostic algorithm based on an artificial neural network to diagnose EMA sensor faults and classify component failures.[17] Della Vedova *et al.* proposed a model-based FDI method for the prognostics of EMAs using genetic algorithms.[18] Ossmann and van der Linden introduce a model-based FDI approach using linear synthesis techniques to detect EMA sensor faults.[19]

In this work, one of the most consolidated strategies for FDI is considered and applied to an EMA-based TVC system. It employs the nullspace approach proposed by Varga[14,20–22] to detect and isolate additive faults affecting the mentioned sensors. The main advantage of the method is that, by using linear synthesis models in LTI (or LPV) form,[16,19,23] it enables the direct decoupling of both disturbances and inputs from the residuals, and provides linear residual generators (or filters) of minimal order, reducing the implementation costs on the final hardware; additionally, uncertainties can also be effectively accounted for. Numerically stable algorithms are used to determine the left nullspace basis of a rational transfer matrix and then synthesize the residual generators. For a TVC system, the consideration of the nozzle load together with the EMA dynamics imply the modeling of the structural compliance between the vehicle skirt and the EMA anchorage point, and the presence of the so-called vehicle-induced loads produced by the rocket motion itself.

It is essential to properly assess the designed filters in fault-free scenarios to not trigger false alarms. To verify the FDI performance, a (nonlinear) physical high-fidelity model has been implemented using the Modelica modeling language and integrated within Simulink®, here adopted as main simulation environment. Robustness against model uncertainties is proven with a small Monte-Carlo simulation campaign in a standalone context, *i.e.* without the full vehicle model. In the same framework, the detection triggering is verified when sensor faults are injected. The filter robustness is lastly assessed using the CALLISTO RLV simulator employing a physical model of the whole rocket (including the aforementioned TVC advanced model), such that the filter is stimulated with representative inputs.

The paper continues in Section 2 with a detailed formulation of the problem and the EMA-based TVC system modelling, including the mechanical load exerted by the rocket engine. Thereafter the mathematical model of an EMA-based TVC system is introduced in Section 3. The FDI synthesis framework is introduced and the application of the nullspace-based synthesis strategy is explained in Section 4, including considerations about isolability of the faults (Section 4.1). In Section 5, the residual generator performance is then assessed in both fault-free and faulty scenarios, and the proposed solution capabilities benchmarked at the example of an RLV mission scenario using a high-fidelity TVC physical model. In Section 6 conclusions are drawn.

2. Problem formulation

To properly modify the engine's thrust vector direction, the TVC actuation system must be able to tilt the engine's nozzle for the correct pointing as commanded by the GNC algorithms. For this reason, the engine is commonly mounted on a gimbal system and maneuvered by two linear actuators in a closed kinematic chain designed to best comply with the EMA load limits, as well as the required speed and maximum displacement operational domains. The actuator therefore must employ an embedded closed-loop control system to be able to track the deflection commands using an appropriate set of sensors. The EMA-based TVC system comprises the following hardware:

1. the engine nozzle, with its structural supports, anchorage points and mechanical joints;

2. a DC power source and the conditioning power electronics;

DOI: 10.13009/EUCASS2023-504

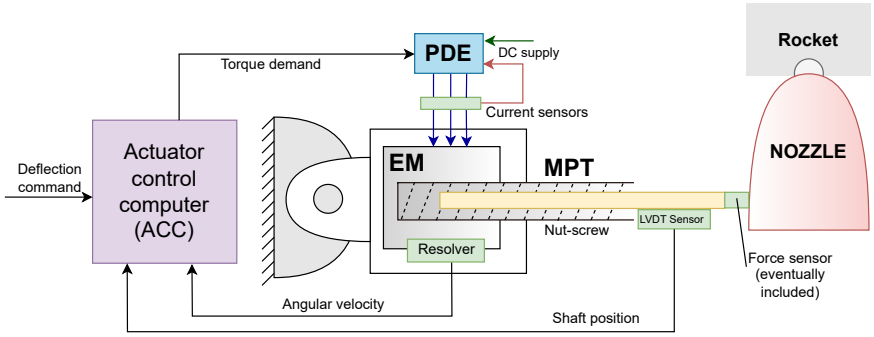

Figure 1: Representation of an EMA-based TVC system architecture.

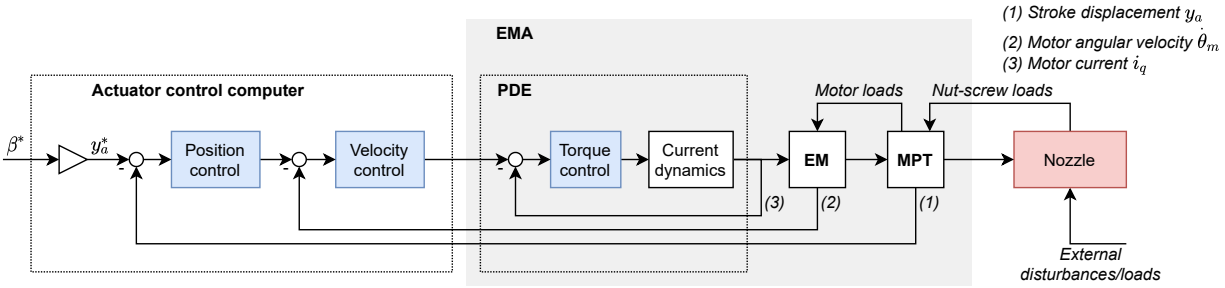

Figure 2: Typical EMA stroke displacement control for TVC deflection command tracking.

3. the embedded actuator control computer (ACC), in charge of controlling the EMA stroke position;
4. two EMAs (one per axis) to physically move the engine nozzle.

At the same time, an EMA is made by different subsystems to produce the required energy transformations and convert the electrical power into mechanical force. Three building components are normally identified:

- the power drive electronics (PDE), which manages the power flow between the electrical supply and actuation system;
- the electric motor (EM), considered as a 3-phase Permanent Magnet Synchronous Motor (PMSM), to obtain a rotational motion from the provided electrical power;
- a mechanical power transmission (MPT) stage to convert the motor rotational motion into a translational motion;
- a set of sensors to be able to control the actuator position, composed by a current sensor, a motor rotational speed sensor, and a stroke displacement position (LVDT) sensor.

The described architecture is synthetically depicted in Figure 1. Note that there exist different MPT configurations: For instance, EMAs may employ a gearbox with appropriate transfer ratios to suitable modify the motor speed/torque domain. Here a direct-drive linear EMA is considered without any gearing element, because of the higher geometrical integration potential, reduced friction and backlash effects, and better efficiency, stiffness and reliability. This solution has also been adopted by the VEGA launch vehicle.[13]

The control system can be freely designed. As a reasonable compromise between simplicity and disturbance rejection properties, typically three nested loops made of PID controllers are employed. Here the following structure is assumed: an outer loop controls the EMA stroke position to obtain the desired nozzle deflection angle as commanded by the GNC system. It must rely on the measurements of a LVDT sensor to produce a suitable velocity reference signal. Another control loop deals with the velocity tracking, exploiting the measurements obtained by the EM sensor(s). Lastly, the innermost loop drives the EM torque control based on the sensed EM current. A depiction of the overall control scheme is shown in Figure 2.

3. Modeling of an Electro-Mechanical Actuator-based TVC system

In this Section an FDI synthesis model of the TVC system is derived. It is assumed that the TVC axes are independent, therefore cross-couplings between the two vectoring directions are not taken into account. The overall TVC architecture

DOI: 10.13009/EUCASS2023-504

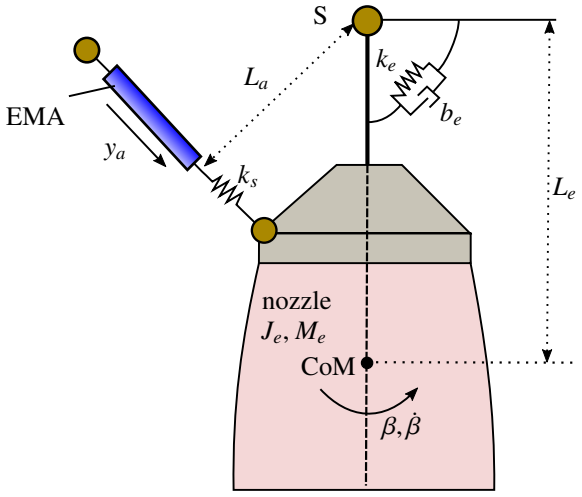

Figure 3: TVC system architecture for linear modeling.

for the development of a linear synthesis model for fault detection is shown in Figure 3. A PDE model is not proposed, since the three-phase inverter switching dynamics lies in a much higher frequency range than the operative EMA one.

3.1 Electric motor modeling

The electric motor balance of torques can be expressed as

$$J_r\ddot{\theta}_m = C_m = C_{em} - C_{m,\text{load}} - C_{\text{loss}}, \tag{1}$$

where J_r is the rotor moment of inertia, θ_m the rotor angular displacement, C_{em} is the electromagnetic torque produced by the motor itself, $C_{m,\text{load}}$ the torque produced by the load connected to the motor, and finally C_{loss} is the torque loss due to the numerous dissipative or disturbance effects, including friction, magnetic losses, hysteresis effects and cogging torque.[24] The latter term is hereafter discarded for the purpose of building a linear model, but reintroduced afterwards in the nonlinear simulation model used for validation. The load on the motor depends on the counteracting force exerted onto the EMA screw; taking L_g as the mechanical (rotational to translational) transmission ratio and introducing a mechanical efficiency factor η_e, the motor load torque can be expressed as

$$C_{m,\text{load}} = L_g F_e / \eta_e, \tag{2}$$

where F_e is the load force acting on the screw, which is detailed in the next Section.

To determine the expression of C_{em}, the stator current equations must be written. For simplicity an isotropic machine is considered. It is known[24,25] that for a PMSM, the three-phase stator and rotor quantities can be transformed into a single rotating reference frame to eliminate the effect of time-varying inductances. This procedure transforms a three-windings machine into a two-phase machine equipped with two windings, which is known as *direct-quadrature-zero* transformation[2]. As such:

$$v_d = R_m i_d + \dot{\Psi}_d - \dot{\theta}_m L_m i_q, \tag{3}$$

$$v_q = R_m i_q + \dot{\Psi}_q + \dot{\theta}_m L_m i_d + \dot{\theta}_m \hat{\Psi}_{pm}, \tag{4}$$

$$\Psi_d = L_m i_d + \hat{\Psi}_{pm}, \tag{5}$$

$$\Psi_q = L_m i_q. \tag{6}$$

where the subscript 'd' and 'q' denote the direct and quadrature axes, respectively; the related currents, voltages and magnetic fluxes are expressed with v, i and Ψ, respectively; L_m and R_m are the winding inductance and resistance, respectively, while $\hat{\Psi}_{pm}$ is a term capturing the magnetic flux related to the permanent magnets. By developing overall machine power equation,[24] one obtains a simplified electromagnetic torque expression as:

$$C_{em} = n_p \hat{\Psi}_{pm} i_q = k_t i_q, \tag{7}$$

[2]Direct axis 'd' fixed with the North of the permanent magnets, and the quadrature 'q' is perpendicular to it.

DOI: 10.13009/EUCASS2023-504

where n_p is the number of the magnetic pole pairs and k_t is known as the motor torque constant. Equation (7) implies that C_{em} depends only on i_q, therefore the relevant current dynamics can be extracted by composing Equations (4) and (6) and by neglecting the cross-coupling terms as:

$$v_q \simeq R_m i_q + L_m \dot{i}_q \implies \dot{i}_q \simeq -\frac{1}{L_m}(R_m i_q + v_q). \tag{8}$$

The input voltage v_q is often regulated by a PI controller with output saturation to respect the physical voltage limits and anti wind-up action for disturbance rejection and to counteract the neglected coupling terms.

3.2 Mechanical power transmission and load modeling

The MPT model simply considers the conversion of the motor torque, angular speed and angular displacement into a force, translational velocity and displacement, as:

$$y_a = L_g \theta_m, \tag{9}$$

$$v_a = L_g \dot{\theta}_m, \tag{10}$$

$$F_a = L_g^{-1} C_m - F_{\text{loss}}, \tag{11}$$

where y_a and v_a are the stroke displacement (from its neutral position) and velocity, F_a the applied force to the load and C_m is from Equation (1). The term F_{loss} contains the dissipation effects and nonlinear characteristics that are in this context ignored. The housing, anchorage and joints stiffness imply a non-negligible dynamic effect which can be captured using a fictitious spring acting between the EMA screw and the load (nozzle). Therefore, this elastic force can be expressed as

$$F_e = k_s(y_a - y_e) \tag{12}$$

where k_s is an equivalent spring coefficient and y_e the translation of the nozzle which, for small deflection angles, can be expressed as

$$y_e = L_a \beta, \tag{13}$$

with β being the nozzle angular deflection for the considered EMA and L_a the actuator lever arm about the gimbaling point.

The nozzle dynamics depends on the displacement produced by the EMA dynamics, it's own inertial effects, but also the effect of another equivalent spring-damper mechanism at the gimbal point with constants k_e and b_e. This means that the dynamics about the gimbal point is

$$\alpha^{-1} \ddot{\beta} = F_e L_a - k_e \beta - b_e \dot{\beta}, \tag{14}$$

where α is a term defining the inverse of the nozzle inertia with respect to the gimbal. Hence

$$\alpha = \frac{1}{J_e + M_e L_e}, \tag{15}$$

with J_e being the nozzle moment of inertia with respect to its center of mass (placed at distance L_e from the gimbal point) and M_e its mass.

3.3 TVC linear model

The whole TVC system model can be finally obtained. Note that, after neglecting C_{loss} and F_{loss}, the equations are linear. The state-space representation can be derived: by considering Equation (8) to describe the current dynamics; by combining Equations (1), (2), (7), (12) and (13) to obtain the motor dynamics; from Equations (12) to (14) for the nozzle dynamics. The sign of β depends on the EMA placement; in this study, it is considered that a positive EMA stroke displacement induces a positive gimbal angle. The resulting state-space system is:

$$\begin{aligned}
\dot{x}_1(t) &= x_2(t) \\
\dot{x}_2(t) &= \alpha \left[-(k_e + L_a^2 k_s) x_1(t) - b_e x_2(t) + k_s L_g L_a x_3(t) \right] \\
\dot{x}_3(t) &= x_4(t) \\
\dot{x}_4(t) &= J_a^{-1} \left[L_g k_s L_a \eta_e^{-1} x_1(t) - L_g^2 k_s \eta_e^{-1} x_3(t) - b_a x_4(t) + k_t x_5(t) + d(t) \right] \\
\dot{x}_5(t) &= {L_m}^{-1} \left[-R_m x_5(t) + u(t) \right]
\end{aligned} \tag{16}$$

DOI: 10.13009/EUCASS2023-504

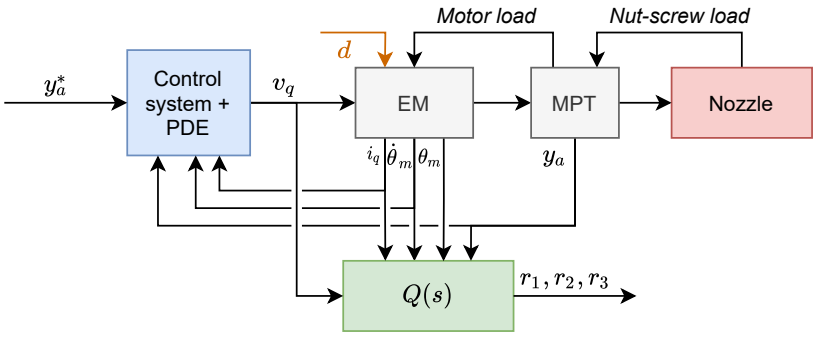

Figure 4: Diagram of the adopted residual generation approach.

$$\begin{aligned} y_1(t) &= x_3(t) \\ y_2(t) &= x_4(t) \\ y_3(t) &= L_g x_3(t) \\ y_4(t) &= x_5(t). \end{aligned} \tag{17}$$

The state vector is therefore $x = [x_1, ..., x_5]^T = [\beta, \dot{\beta}, \theta_m, \dot{\theta}_m, i_q]^T$. Note that all the moments of inertia are expressed with respect to the gimbal point S. The outputs depend on the available sensors, which are the motor angular displacement, the motor angular rate, the stroke displacement and the motor current. Therefore the output vector is $y = [y_1, ..., y_4]^T = [\theta_m, \dot{\theta}_m, y_a, i_q]^T$. The inputs are the motor quadrature voltage ($u = v_q$) and an additive term including the disturbance $d(t)$ acting on the TVC. The latter correspond to the vehicle-induced loads, hence the reaction forces and torques applied at the gimbal point as consequence of the rocket motion. The linear model can be rewritten in the classic matrix form:

$$\begin{aligned} \dot{x}(t) &= Ax(t) + b_u u(t) + b_d d(t) \\ y(t) &= Cx(t) \end{aligned} \tag{18}$$

Remark 1. Further disturbances to the TVC dynamics are, in this work, not considered. They may include, for instance, aerodynamic effects acting on the nozzle. Their magnitude is here considered negligible with respect to the vehicle-induced loads.

3.4 Residual generator synthesis model

The fault detection process focuses on the sensors whose degradation can affect the closed-loop performance. Therefore, the motor angle θ_m is used as available measurement from the residual generator, but only motor velocity, motor current and actuator position are monitored for additive faults. As such, the outputs of Equation (18), must be augmented with the fault inputs:

$$\begin{aligned} \dot{x}(t) &= Ax(t) + b_u u(t) + b_d d(t) \\ y(t) &= Cx(t) + f(t). \end{aligned} \tag{19}$$

where the vector $f(t) = [0, f_1(t), f_2(t), f_3(t)]^T$ is consists of generic input signals; this implies that the synthesis is not limited to specific fault types.

4. FDI residual generator synthesis

In the state space expressed in Equation (19), the load $d(t)$ acting on the nozzle, and thus indirectly affecting the motor dynamics, is considered as unknown disturbance that has to be perfectly decoupled from the outputted residual signals. To simplify the synthesis procedure description, the augmented state-space can be rewritten in the Laplace domain in input-output form as

$$\mathbf{y}(s) = G_u(s)\mathbf{u}(s) + G_d(s)\mathbf{d}(s) + G_f(s)\mathbf{f}(s), \tag{20}$$

DOI: 10.13009/EUCASS2023-504

where the quantities $\mathbf{y}, \mathbf{u}, \mathbf{d}, \mathbf{f}$ have the same meaning as before, but written in the Laplace domain, whereas G_u, G_d and G_f the derived transfer function matrices. In the case under study, G_f has dimensionality 4×3 and has no dynamics (hence constant), since the faults directly affect the output. On the other hand, G_u and G_d have dimension 4×1. The fault detection and isolation problem requires a residual generator which can be written as

$$\mathbf{r}(s) = Q(s) \begin{bmatrix} \mathbf{y}(s) \\ \mathbf{u}(s) \end{bmatrix}, \tag{21}$$

where $\mathbf{r}(s)$ are the residual signals (in Laplace domain) and $Q(s)$ the filter to be synthesized, which must be stable (only poles with negative real part) and proper. The fault detection problem is addressed by producing residuals

$$r(t) = \begin{bmatrix} r_1(t) \\ r_2(t) \\ r_3(t) \end{bmatrix} \tag{22}$$

different from zero whenever a fault occurs. The residuals are then compared with a threshold to determine if the amplitude of the residual is "large enough" to avoid false alarms. When the residual vector is sensitive to all faults, the *complete fault detectability* property is achieved. Furthermore, when faults enter in the system dynamics as signals with a clear frequency signature, *i.e.* there exist a set of frequencies (including zero) that defines the fault signals (for example to detect bias or oscillatory faults), then the *strong fault detectability* property is desirable. These properties are formalized in the next Section. On the other hand, isolability concerns the location of the fault, hence the determination of the presence of a specific fault by associating the raise (or non raise) of a specific residual signal r_j (or more residuals) with a specific fault f_j. Normally, it is desirable that multiple occurring faults can be detected at the same time without altering the isolation capability: when this happens, the property is be called *strong fault isolation*.

Remark 2. Another problem formulation could include the vehicle-induced load disturbances $d(t)$ as an additional fictitious control input. This is considered an option because the loads can be computed knowing the vehicle states. However, the load computation depends on both TVC deflection values, but the latter are normally determined directly from y_a or θ_m measurement. In presence of faults on one of these two quantities (especially on θ_m that is not monitored), also the load computation would lead to wrong results, thus jeopardizing the FDI system.

4.1 Detectability and isolability analysis

We desire *strong complete fault detectability* and *strong fault isolability* properties. It is convenient to rewrite Equation (21) after substituting Equation (20):

$$\mathbf{r}(s) = Q(s) \begin{bmatrix} G_u(s) & G_d(s) & G_f(s) \\ 1 & 0 & 0 \end{bmatrix} \begin{bmatrix} \mathbf{u}(s) \\ \mathbf{d}(s) \\ \mathbf{f}(s) \end{bmatrix}. \tag{23}$$

Complete fault detectability can be achieved[22] if and only if:

$$\operatorname{rank} \begin{bmatrix} G_d(s) & G_{f_j}(s) \end{bmatrix} > \operatorname{rank} \left(G_d(s) \right) \tag{24}$$

with $j \in [1, 2, 3]$ representing the j-th column of the related matrix. This is generally fulfilled whenever the output measurements are more than the disturbance inputs, which is the case of the system under study. For strong fault detectability a set of complex frequencies of interest Ω must be defined. Only the set $\Omega = \{0\}$ is considered, thus detectability of constant faults (*i.e.* biases) is checked. Let us define:

$$G_{e_j}(s) := \begin{bmatrix} G_{f_j}(s) & G_u(s) & G_d(s) \\ 0 & 1 & 0 \end{bmatrix} \tag{25}$$

and

$$\bar{G}_{e_j}(s) = \begin{bmatrix} G_{e_j}(s) \\ I_{1\times 3} \end{bmatrix}, \tag{26}$$

with $I_{1\times 3}$ being a truncated identity matrix $[1, 0, 0]$. Strong fault detectability is achieved when every fault f_j is detactable and when the matrix G_{e_j} has the same zero structure of $\bar{G}_{e_j}$ for every $s \in \Omega$. This latter condition is also verified for the system in (19).

DOI: 10.13009/EUCASS2023-504

Table 1: Detectability and isolability of faults within a EMA-based TVC system based on different measurements and fault configurations.

Measurement and fault configurations			Detectability		Isolability		
			Complete	Strong	No	Weak	Strong
#1	Outputs:	$[\theta_m, \dot{\theta}_m, y_a, i_q]$	✓	✓			✓
	Faults:	$[\dot{\theta}_m, y_a, i_q]$					
#2	Outputs:	$[\dot{\theta}_m, y_a, i_q]$	✓	✓	✓		
	Faults:	$[\dot{\theta}_m, y_a, i_q]$					
#3	Outputs:	$[\dot{\theta}_m, y_a, i_q, F_e]$	✓	✓			✓
	Faults:	$[\dot{\theta}_m, y_a, i_q]$					
#4	Outputs:	$[\dot{\theta}_m, y_a, i_q, F_e]$	✓	✓		✓	
	Faults:	$[\dot{\theta}_m, y_a, i_q, F_e]$					
#5	Outputs:	$[\theta_m, \dot{\theta}_m, y_a, i_q, F_e]$	✓	✓			✓
	Faults:	$[\dot{\theta}_m, y_a, i_q, F_e]$					

For strong fault isolability one can define the fault signature matrix S where each element (k-th column, i-th row) is populated as follows:

$$S_{k,i} = \begin{cases} 1 & \text{if } R^j_{f_i}(0) \neq 0 \\ 0 & \text{if } R^j_{f_i}(s) = 0 \\ -1 & \text{if } R^j_{f_i}(0) = 0 \wedge R^j_{f_i}(s) \neq 0, \end{cases} \tag{27}$$

where $R^j_{f_i}$ is the transfer function from i-th fault to j-th residual. When an entry is '1', it means that when a fault occurs, the steady value of the residual output is nonzero, otherwise the residual displays the fault only "temporarily" and then the entry is '-1'. In case the residual is not affected by the fault at all, then '0' is set. Clearly the ideal case is when $S = I_{3\times3}$, which occurs only when:[22]

$$\text{rank}\begin{bmatrix} G_d(s) & G_f(s) \end{bmatrix} = \text{rank}(G_d(s)) + m_f, \tag{28}$$

with m_f being the number of outputs. For the system in (19), Equation (28) can be trivially verified.

However, it is natural to wonder if this is the only possible measurements-faults combination. For example, if θ_m output was also monitored for faults, could the strong fault detectability and isolability properties be kept? This is also of great relevance if $\dot{\theta}_m$ is obtained by differentiating θ_m. In this case, it may be possible that a fault affecting θ_m also affects $\dot{\theta}_m$ signal. Therefore, it is advantageous to define which combinations of measurements and input faults are feasible for *strong* FDI. This analysis is summarized in Table 1. Case #1 represents the situation so far investigated; Case #2 is concerned with the eventuality that θ_m measurements are removed from the problem formulation. In this case, it is not possible to achieve fault isolation at all. The only residual completely unaffected by this change is the motor current; the other residuals are coupled. As such, there exist no such residual that does not get triggered by a fault on $\dot{\theta}_m$ and not on y_a, and vice-versa. Case #3 explores a new possibility: it is not rare that a TVC system includes a force sensor between the EMA and the nozzle, *i.e.* at the anchorage point. This is described by Renault[26] and can be effectively employed to augment the EMA control system to dampen the nozzle oscillations. When this quantity is available, it can be added in the outputs in Equation (17) as

$$y_5 = F_e = -L_a k_s x_1 + L_g k_s x_3 \tag{29}$$

and consequently included in the FDI problem formulation. This restores the strong fault isolation property of Case #2. If also faults on the force sensor are to be determined, the latter property is lost again. In this case weak fault isolability can be achieved, up to one fault can be isolated (Case #4). If from Case #4 we relax the θ_m output elimination assumption, an arbitrary number of faults can be detected and isolated again, since another measurement is available (Case #5).

Remark 3. The presence of the disturbance input d makes a great difference in the fault detectability and isolability properties. Excluding it from the problem formulation could be beneficial only when its amplitude is relatively small with respect to the impact it has on the overall dynamics. In the TVC case, the vehicle-induced loads are definitely not negligible. This is also why, during the control system design of a rocket, the so-called tail-wag-dog effect is especially

DOI: 10.13009/EUCASS2023-504

taken into account to counteract the dynamics from the nozzle swinging. This is indeed the dual effect of the described TVC vehicle-induced loads.

4.2 The nullspace method

The nullspace method is considered in this work as approach to derive a suitable dynamic filter for the computation of the residual signals. This is extensively described by Varga.[22] Solving the the Exact Fault Detection and Isolation Problem (EFDIP) is hereafter considered. It allows the decoupling of both disturbances and inputs, and provides filters of minimal order, a desirable property for the final implementation into the hardware and for disturbance rejection. It is composed by three steps, at the end of which the filter $Q(s)$ gets updated as $Q(s) \leftarrow Q_K(s)...Q_1(s)$ with K being the step index.

The first step is to determine a basic fault detection filter. This basic filter can be seen as a composition of three different dynamical systems, each dealing with one fault as

$$Q(s) = [Q^1(s), Q^2(s), Q^3(s)]^T. \tag{30}$$

For each sub-filter to achieve perfect decoupling of inputs, disturbance and all the "non-related" faults, the following condition obtained from Equation (23) must be fulfilled:

$$Q^i(s)\begin{bmatrix} G_u(s) & G_d(s) & \tilde{G}_{f,i}(s) \\ 1 & 0 & 0 \end{bmatrix} := Q^i(s)G_e(s) = 0, \tag{31}$$

where $\tilde{G}_{f,i}(s)$ is a fault transfer matrix where all faults with index different than i have been excluded. Equation (31) means imposing that $Q^i(s)$ must be a left-annihilator of $G_e(s)$. This implies that it can be solved by determining a left nullspace basis of $G_e(s)$ which is able to fulfill the decoupling conditions while allowing the i-th filter to be affected by the i-th fault.

The second step is meant to reduce the order of $Q(s)$ by selecting a suitable transfer function matrix $Q_2(s)$ that makes $Q_2(s)Q(s)$ have the least (McMillan) degree. The idea is to try out different polynomial basis vector combinations (with different degrees) iteratively, to make sure that the fault becomes visible with the least order one.

The last step is to eventually stabilize the filter and impose the desired dynamics. Therefore, a proper and invertible $Q_3(s)$ is designed using a left coprime factorization, such that the resulting final filter $Q_3(s)Q(s)$ has the desired dynamics. In this case, it has been imposed that the poles of the filter are set to -10, as a good compromise between detection speed and filtering eventual high frequency measurement noise.

4.3 Analysis of the synthesized residual generators

The filter $Q^1(s)$ is in charge of detecting faults on the motor angular velocity. It is a first order transfer function that compares the filtered and differentiated motor position with the measured angular velocity. This means that the filter has a zero in $s = 0$. On the other hand, $Q^2(s)$ is a constant filter directly comparing the motor position with the stroke position multiplied by a gain. The additional plant output θ_m (not subject to faults) is basically acting as hardware redundancy to directly check y_a. Lastly, $Q^3(s)$ is again a first order filter; it must be noticed that in this case the pole could not be imposed, because the residual is obtained by subtracting the dynamic effect of a voltage input in terms of predicted current, to the current measurement itself. In conclusion, the dynamics is dictated by the current one, as per Equation (8). Therefore, the overall filter $Q(s)$ is second order when assembling all the filters together. For the other cases considered in Section 4.1, namely #3 and #6, the structure of the filter becomes slightly different, but the order of each individual sub-filters never overcomes three. Hereafter, only Case #1 is considered.

5. Simulation results

In this Section the performance of the FDI filter is assessed. The simulation setup includes a nonlinear high-fidelity TVC model developed using Modelica, an open-souce multi-physics acausal modeling language. This has several advantages: *a*) it enables a clear representation of physical meaning within an object-oriented structure; *b*) a free Modelica Standard Library (MSL) exists[27] for the creation of multibody models, entailing several benefits for the TVC modeling; *c*) advanced friction models together with backlash effects can be obtained.[25] The TVC model employed here is included in DLR's VLVLib.[28,29] In the Modelica model, the following effects are included (grouped within F_{loss} in Equation (11)):

DOI: 10.13009/EUCASS2023-504

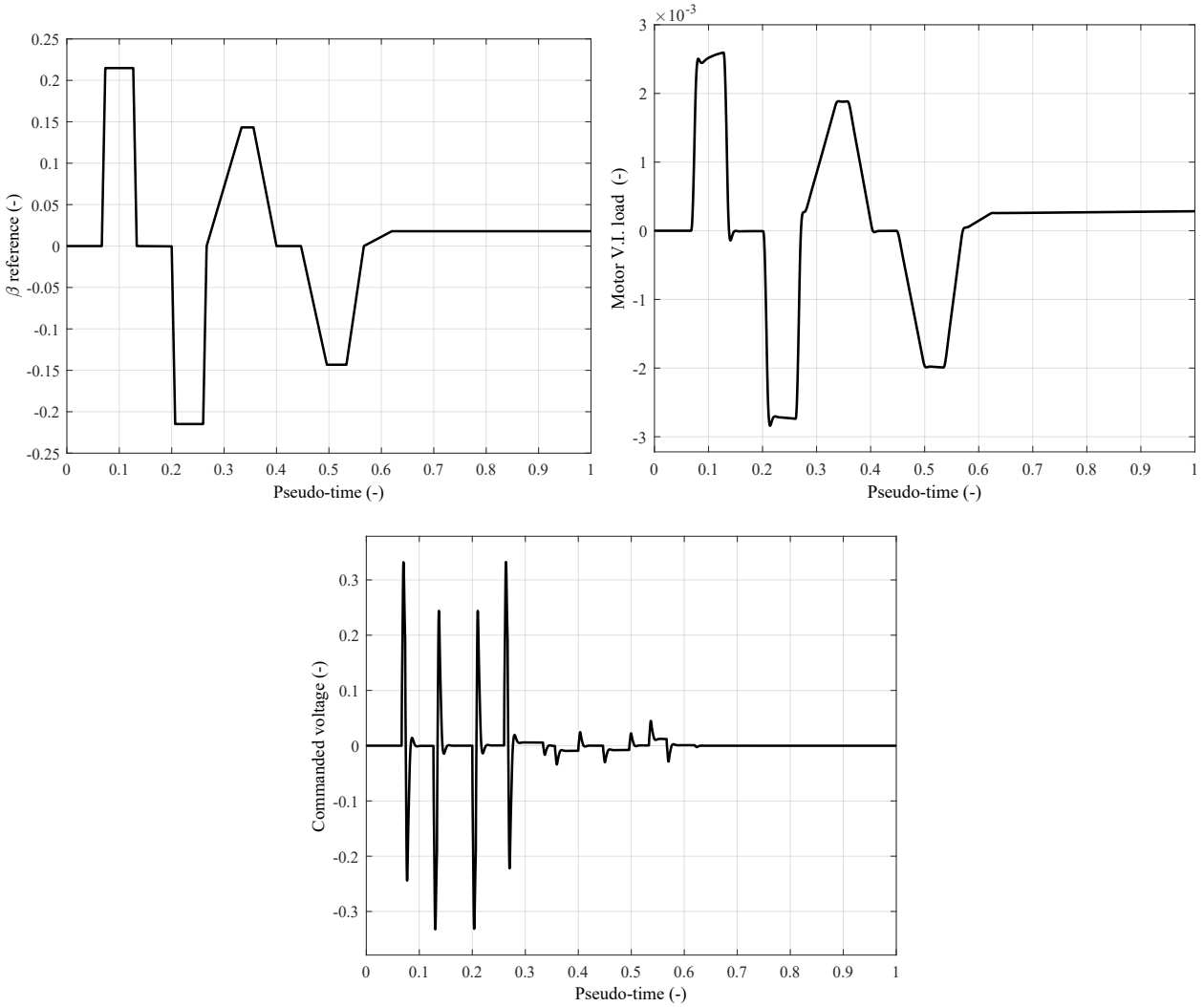

Figure 5: Reference signals for the fault-free Monte-Carlo campaign; motor load and voltage signals refer to the unperturbed case.

- a load-dependent friction model: it includes several nonlinear effects, like the Coulomb and Stribeck friction, as well as a viscous (linearly velocity-dependent) component. In addition, it is known[30,31] that the load alters the friction properties. In this work, this aspect has been considered as well, *cf.* Marè *et al.*[30] and Farì *et al.*[25]

- backlash effect: it is known that EMAs are subject to backlash, hence a "loss of motion" happening while the mechanical components are not in contact. Normally, in modern EMAs, this effect is generally small, but it has the potential of degrading the FDI performance;

- the EMA screw mass, that adds an additional small load onto the motor.

At the same time, the EM model includes the following effects (grouped within C_{loss} in Equation (1)):

- a friction model, that includes the Coulomb and Stribeck friction, as well as a viscous (linearly velocity-dependent) component;

- the hysteresis losses and cogging torque effect.

This nonlinear model is included in all the following setups: at first, the FDI robustness is assessed in a fault-free scenario. Then, it is shown that the filter reacts and correctly responds to the injected faults. Lastly, the full end-to-end mission of CALLISTO VTVL RLV[32] is used to prove that, in a fault-free situation, the FDI filter has a good performance when solicited by representative inputs and disturbance.

DOI: 10.13009/EUCASS2023-504

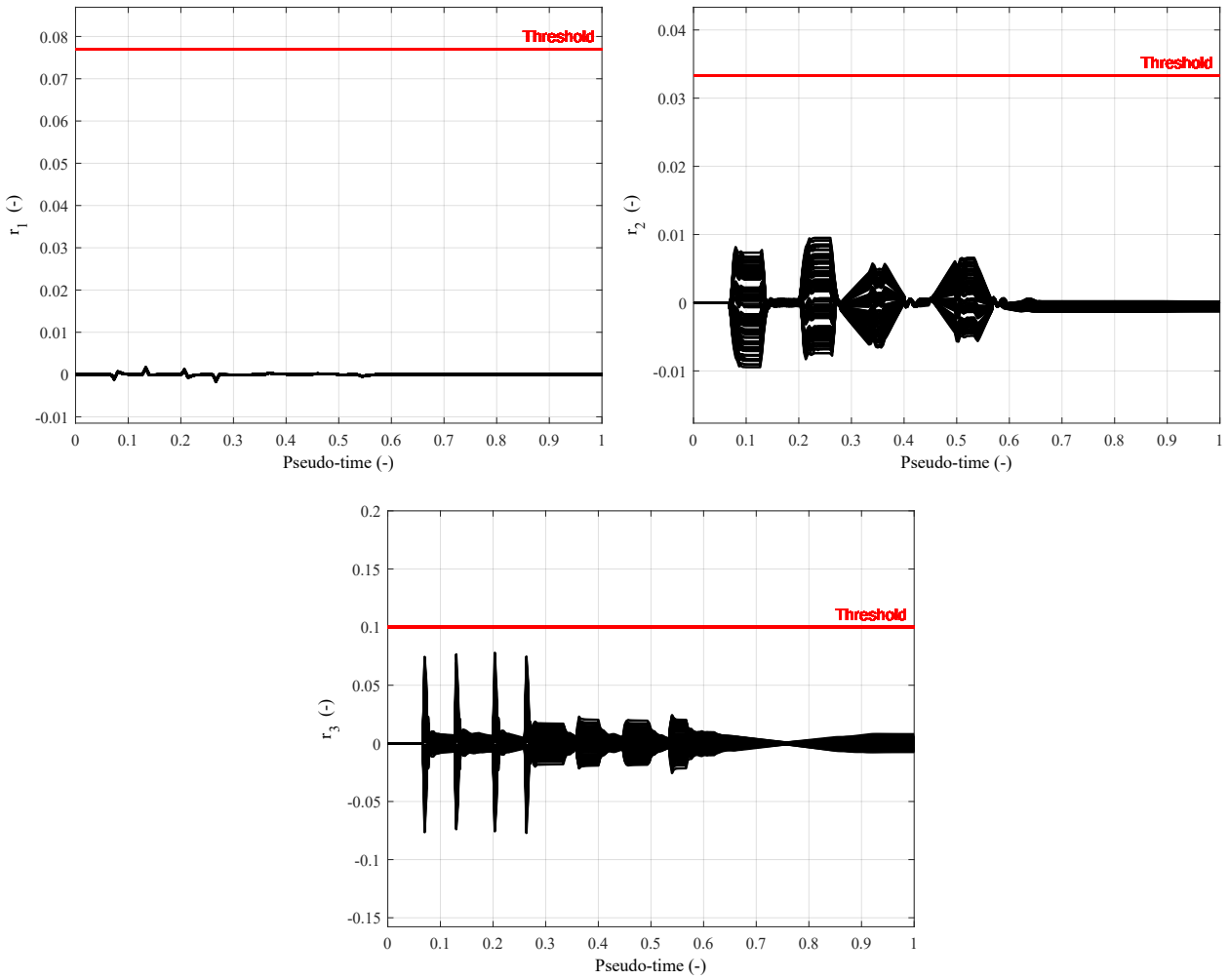

Figure 6: Residual signals in a fault-free Monte-Carlo simulation campaign using a high-fidelity TVC model.

5.1 Fault-free scenario

At first, the case where no faults are present is discussed, as it is essential to prove that the performance of the FDI filter are robust in the nominal case (with vehicle-induced disturbances), but also against the aforementioned unmodeled effects and parametric uncertainties. The TVC model with the EMA nonlinear dynamics is compiled as a Functional Mock-up Unit (FMU) and integrated within a Simulink® simulator. A Monte-Carlo campaign of 100 runs is then performed; all parameters have been perturbed with a uniform distribution in the range of 10%-20% of their nominal value. The injected TVC deflection angle reference is reported in Figure 5, together with the reference stroke displacement command, the motor loads and the commanded voltage in the nominal case. Note that the plots have been normalized. The vehicle-induced loads acting on the TVC are extracted from a high-fidelity simulation of the launch phase and injected in the simulation. They act exclusively when the β deflection angle is different than zero; this is a normal consequence of the fact that the action-reaction forces between the vehicle main body and the nozzle due to the vehicle acceleration are present only if the center of mass of the nozzle is not longitudinally aligned with the one of the main body.

The FDI performance depends upon the choice of suitable thresholds for the residuals. They are not uniquely defined since they depend on the amplitude of faults which are considered relevant. The thresholds are selected to correspond to 3-10% of the normal operation range of the motor velocity, stroke displacement and motor current.

Figure 6 shows the three resulting residual signals. As expected they are not zero as applied to a nonlinear model with parameter perturbations. Despite that, they remain lower than the selected thresholds. It can be seen how the current signal is the one more close to its thresholds and therefore has to be treated with care, for example when trying to estimate the fault amplitude.

DOI: 10.13009/EUCASS2023-504

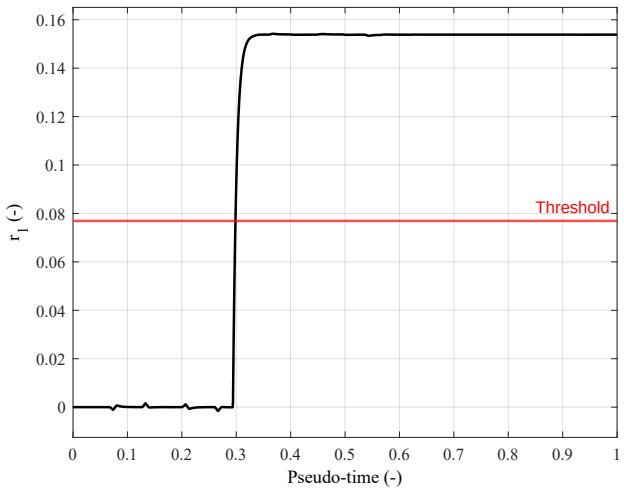

(a) Monte-Carlo campaign with a bias fault on $\dot{\theta}_m$ sensor.

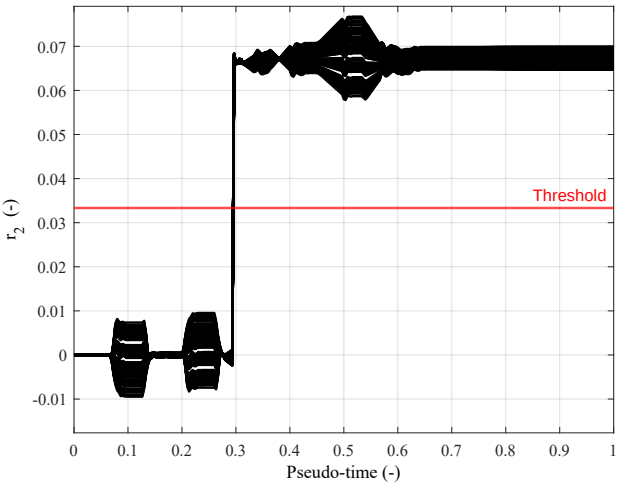

(b) Monte-Carlo campaign with a bias fault on y_a sensor.

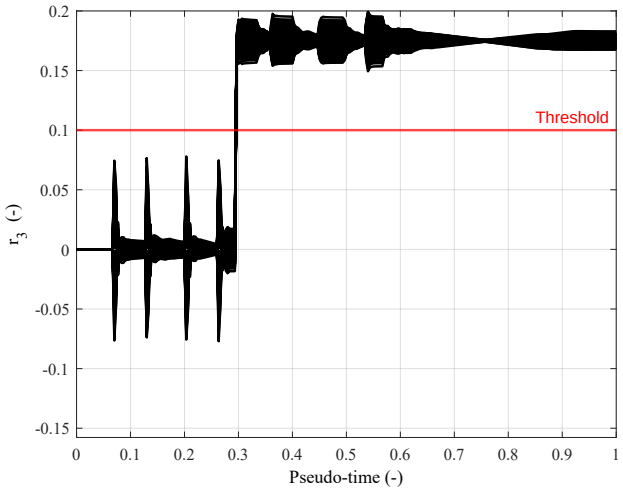

(c) Monte-Carlo campaign with a bias fault on i_q sensor.

Figure 7: Residual signals in presence of a bias fault using a high-fidelity TVC model.

5.2 Fault simulations

For faults injection, the same simulation setup is used. Three different Monte-Carlo simulation campaigns (100 runs) have been ran, each with a bias fault introduced at about one third of the overall simulation time into $\dot{\theta}_m$, y_a and i_q measurements, respectively. The results are depicted in Figure 7. It can be noticed that r_1 residual behaves as a first order system, in accordance to what expected. The stroke displacement residual r_2 instead has no dynamics. Lastly, the motor current residual r_3 has the form of a step. For the reasons explained in Section 4.3 that the voltage dynamics is fast, the result is a filter with a very small time constant. In all cases the selected threshold is exceeded by at least 20%, which is an acceptable robustness margin with respect to the chosen thresholds. Note that for the achieved strong isolation property, the residual magnitude would have not differed substantially if the fault was injected in the same simulation.

The most important consequence for faults affecting EMA sensors is that closed-loop performance can be heavily degraded. Figure 8 shows the case of an EMA step position command (implying a step in y_a) at about one fourth of the pseudo-time and a bias fault affecting y_a sensor at about half the simulation time. It can be seen that the EMA controller immediately reacts to the fault by adjusting the voltage output and compensate for the bias. However, this means that the actual position of the stroke is different than the one supposed by the flight control system. In turn, depending on the TVC lever arm L_a, this can result in a very degraded tracking of the β^* TVC deflection commands for vehicle control.

DOI: 10.13009/EUCASS2023-504

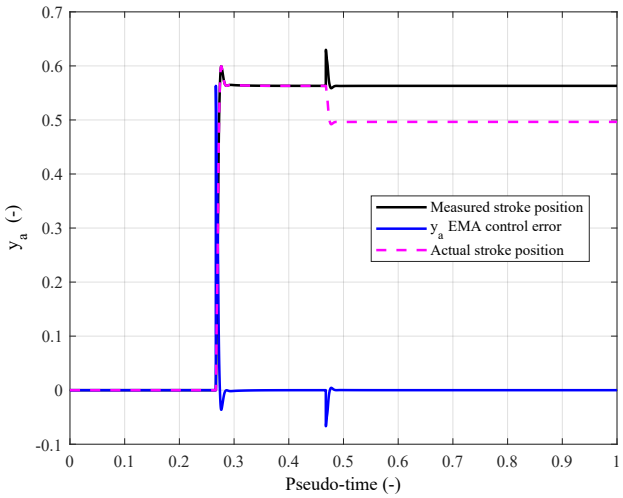

Figure 8: Consequence at closed-loop TVC control system level after a fault affecting y_a.

5.3 Fault-free scenario in an end-to-end RLV mission simulation

To confirm that the FDI filter can be applied to the scenario of a reusable launch vehicle, the full end-to-end high-fidelity CALLISTO simulator is employed and ran contextually with the residual generator. Therefore, the filter is engaged with the inputs and disturbance of the CALLISTO vehicle, which undergoes the flight phases ascent, boostback, aerodynamic re-entry and the engine re-ignition for the final landing and touchdown. The simulation is conducted with both vehicle and TVC nominal parameters. The advanced model adopted previously is here included for both TVC directions. The vehicle is modeled using Modelica as well: this includes the vehicle structural dry mass and several masses representing the propulsion fluidics masses (with time-varying position as the fuel is depleted). This makes it a multibody model; note that, with such a modeling, the two EMAs may slightly disturb each other during simultaneous thrust vectoring. Figure 9 shows the final results for one of the two TVC actuators (the other would exhibit as very similar). The good residual performance is confirmed for a fault-free case, and it is shown that the filter is almost insensitive to the vehicle dynamics and that local monitoring is not affected by the vehicle-induced loads which have been sufficiently decoupled. A Monte-Carlo analysis is here not performed because the simulation computational burden is very high, thus requires a considerable amount of time. This aspect will be taken into account in future works.

6. Conclusions

This paper presented an effective methodology for the synthesis of a fault detection and isolation filter targeting the sensors included in the electro-mechanical actuators maneuvering a TVC system. Assessing performance degradation to the TVC closed-loop control system is essential to secure reliable performance and have successful missions. Exploiting this additional information can lead to in-flight control laws adjustment to accommodate the fault, or post-flight analysis, inspection and maintenance to keep the actuator fully operative.

An analysis of fault detectability and isolability of the faults affecting the motor angular velocity sensor, the stroke displacement sensor and the motor current sensor has been performed. It has been shown that a measurement of the motor angle (*e.g.* via a angular resolver) enables *complete strong fault detectability* and *strong fault isolability* of the sensors, whose measurements are employed in the EMA control system. Scenarios with different measurements/fault-requirements combinations have been discussed. The nullspace method for filter synthesis has proven effective for successfully decoupling the plant input, measurement and disturbance (vehicle-induced loads) from the residual signal. The performance of the filter has been tested in fault-free scenarios with a Monte-Carlo campaign and robustness has been successfully proved in all cases in both a standalone simulator and applied to a full end-to-end reusable launch vehicle mission. It has been shown how the residual correctly identifies the fault occurrence when sensor biases are artificially injected.

Acknowledgments

This research is funded by the European Space Agency (ESA) – Ph.D. grant nr. 4000134582/21/NL/GLC – and the German Aerospace Center (DLR).

DOI: 10.13009/EUCASS2023-504

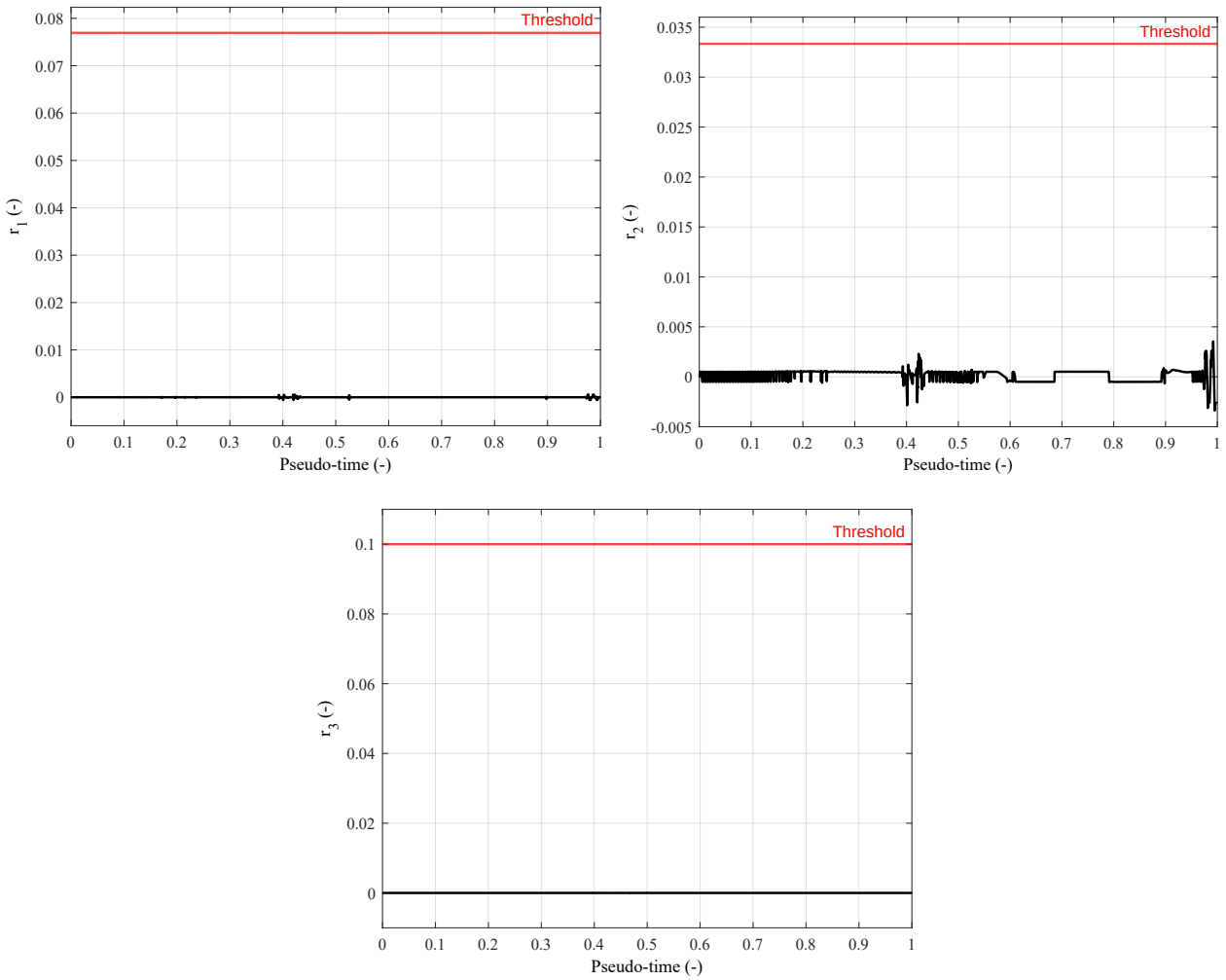

Figure 9: Fault-free residual signals in an end-to-end high-fidelity simulation of a VTVL RLV mission.

References

[1] Etienne Dumont, Michel Illig, Shinji Ishimoto, Christophe Chavagnac, Yasuhiro Saito, Sven Krummen, Silas Eichel, Hauke Martens, Sofia Giagkozoglou, Janis Sebastian Häseker, Tobias Ecker, Josef Klevanski, Felix Krziwanie, Waldemar Rotärmel, Silvio Schröder, Anton Schneider, Christian Grimm, Svenja Woicke, Marco Sagliano, Markus Schlotterer, Markus Markgraf, Benjamin Braun, Moritz Aicher, Lale Evrim Briese, Ivaylo Petkov, Johannes Riehmer, and Bodo Reimann. CALLISTO: A Prototype Paving the Way for Reusable Launch Vehicles in Europe and Japan. In *73rd International Astronautical Congress (IAC)*, Paris, France, September 2022.

[2] Etienne Dumont, Tobias Ecker, Christophe Chavagnac, Lars Witte, Jens Windelberg, Josef Klevanski, and Sofia Giagkozoglou. CALLISTO - Reusable VTVL launcher first stage demonstrator. In *Space Propulsion Conference 2018*, Seville, Spain, May 2018.

[3] Charles Bertorello, Olivier Gogdetb, Jérôme Breteauc, Yann Tincelind, Elisa Cliquet-Moreno, Emmanuel Coletti, and Sorya Bensalem. Themis Demonstration Programme. In *73rd International Astronautical Congress (IAC)*, Paris, France, 2022. International Astronautical Federation (IAF).

[4] Ansgar Marwege, Josef Klevanski, Johannes Riehmer, Daniel Kirchheck, Sebastian Karl, Davide Bonetti, J. Vos, Matthew Jevons, Anett Krammer, and João Carvalho. Retro Propulsion Assisted Landing Technologies (RETALT): Current Status and Outlook of the EU Funded Project on Reusable Launch Vehicles. In *70th International Astronautical Congress (IAC)*, Washington D.C., United States, October 2019.

DOI: 10.13009/EUCASS2023-504

[5] Brian Bjelde, Peter Capozzoli, and Gwynne Shotwell. The SpaceX Falcon 1 Launch Vehicle Flight 3 Results, Future Developments, and Falcon 9. In *Proceedings of the International Astronautical Congress*. International Astronautical Federation, 2008.

[6] Rocket Lab. Launch - Payload Users Guide 6.5, 2020.

[7] Jean-Charles Maré and Jian Fu. Review on signal-by-wire and power-by-wire actuation for more electric aircraft. *Chinese Journal of Aeronautics*, 30(3):857–870, June 2017.

[8] A. Garcia, I. Cusido, J.A. Rosero, J.A. Ortega, and L. Romeral. Reliable electro-mechanical actuators in aircraft. *IEEE Aerospace and Electronic Systems Magazine*, 23(8):19–25, August 2008.

[9] Guan Qiao, Geng Liu, Zhenghong Shi, Yawen Wang, Shangjun Ma, and Teik C Lim. A review of electromechanical actuators for More/All Electric aircraft systems. *Proceedings of the Institution of Mechanical Engineers, Part C: Journal of Mechanical Engineering Science*, 232(22):4128–4151, November 2018.

[10] Lisa B. Bates and David T. Young. Developmental Testing of Electric Thrust Vector Control Systems for Manned Launch Vehicle Applications. In *41st Aerospace Mechanisms Symposium*, Pasadena, CA, May 2012.

[11] Cesare Carnevale and Pier Resta. Vega Electromechanical Thrust Vector Control Development. In *43rd AIAA/ASME/SAE/ASEE Joint Propulsion Conference Exhibit*, Cincinnati, OH, July 2007. American Institute of Aeronautics and Astronautics.

[12] Tillo Vanthuyne. An electrical thrust vector control system for the VEGA launcher. In *13th European Space Mechanisms and Tribology Symposium*, Vienna, Austria, 2009.

[13] Gael Dee, Tillo Vanthuyne, Alessandro Potini, Ignasi Pardos, and Guerric De Crombrugghe. Electromechanical thrust vector control systems for the VEGA-C launcher. In *8th European Conference For Aeronautics And Space Sciences (EUCASS)*, Madrid, Spain, 2019.

[14] Daniel Ossmann, Hans-Dieter Joos, and Philippe Goupil. Enhanced Sensor Monitoring to Maintain Optimal Aircraft Handling in Case of Faults. *Journal of Guidance, Control, and Dynamics*, 40(12):3127–3137, 2017.

[15] Daniel Ossmann. Enhanced Fault Detection and Isolation in Modern Flight Actuators. In *3rd Australian Control Conference, AUCC 2013*, November 2013.

[16] Andreas Varga, Simon Hecker, and Daniel Ossmann. Diagnosis of actuator faults using LPV-gain scheduling techniques. In *AIAA Guidance, Navigation, and Control Conference*, Portland, Oregon, August 2011. American Institute of Aeronautics and Astronautics.

[17] Edward Balaban, Prasun Bansal, Paul Stoelting, Abhinav Saxena, Kai F. Goebel, and Simon Curran. A diagnostic approach for electro-mechanical actuators in aerospace systems. In *2009 IEEE Aerospace Conference*, pages 1–13, Big Sky, MT, USA, March 2009. IEEE.

[18] Matteo D. L. Dalla Vedova, Alfio Germanà, Pier Carlo Berri, and Paolo Maggiore. Model-Based Fault Detection and Identification for Prognostics of Electromechanical Actuators Using Genetic Algorithms. *Aerospace*, 6(9):94, September 2019.

[19] Daniel Ossmann and Franciscus L. J. van der Linden. Advanced sensor fault detection and isolation for electromechanical flight actuators. In *2015 NASA/ESA Conference on Adaptive Hardware and Systems (AHS)*, pages 1–8, Montreal, QC, June 2015. IEEE.

[20] A. Varga. The nullspace method - a unifying paradigm to fault detection. In *Proceedings of the 48h IEEE Conference on Decision and Control (CDC) Held Jointly with 2009 28th Chinese Control Conference*, pages 6964–6969, December 2009.

[21] Andreas Varga. New computational paradigms in solving fault detection and isolation problems. *IFAC Proceedings Volumes*, 45(20):983–998, January 2012.

[22] Andreas Varga. *Solving Fault Diagnosis Problems*, volume 84 of *Studies in Systems, Decision and Control*. Springer International Publishing, Cham, 2017.

[23] Andreas Varga and Daniel Ossmann. LPV model-based robust diagnosis of flight actuator faults. *Control Engineering Practice*, 31:135–147, October 2014.

DOI: 10.13009/EUCASS2023-504

[24] R. Krishnan. *Permanent Magnet Synchronous and Brushless DC Motor Drives*. CRC Press, 1 edition, December 2017.

[25] Stefano Farì, David Seelbinder, Stephan Theil, Pedro Simplicio, and Samir Bennani. Physical modeling and simulation of electro-mechanical actuator-based TVC systems for reusable launch vehicles. *(Under review)*, 2023.

[26] Cédric Renault. Usefulness of a force feedback on electromechanical actuator. In *6th International ESA Conference on Guidance, Navigation and Control Systems*, Loutraki, Greece, 2005.

[27] Martin Otter, Hilding Elmqvist, and Sven Erik Mattsson. The New Modelica MultiBody Library. In *3rd International Modelica Conference*, page 21, 2003.

[28] Stefano Farì. The Vertical Landing Vehicles Library (VLVLib): A Modelica-based approach to high-fidelity simulation and verification of GNC systems for reusable rockets. In *73rd International Astronautical Congress (IAC)*, Paris, France, 2022. International Astronautical Federation.

[29] Stefano Farì, David Seelbinder, and Stephan Theil. Advanced GNC-oriented modeling and simulation of Vertical Landing vehicles with fuel slosh dynamics. *Acta Astronautica*, 204:294–306, December 2022.

[30] Jean-Charles Mare. Friction modelling and simulation at system level: A practical view for the designer. *Proceedings of the Institution of Mechanical Engineers, Part I: Journal of Systems and Control Engineering*, 226(6):728–741, July 2012.

[31] Jean-Charles Maré. Practical Considerations in the Modelling and Simulation of Electromechanical Actuators. *Actuators*, 9(4):94, December 2020.

[32] Michel Illig, Shinji Ishimoto, and Etienne Dumont. CALLISTO, a demonstrator for reusable launchers. In *9th European Conference For Aeronautics And Space Sciences (EUCASS)*, 2022.